Available online at www.sciencedirect.com
ScienceDirect
Journal of Solid State Chemistry 180 (2007) 1365–1371
JOURNAL OF SOLID STATE CHEMISTRY
www.elsevier.com/locate/jssc

Synthesis and VUV–UV spectroscopic properties of rare earth borosilicate oxyapatite: $RE_5Si_2BO_{13}$: Ln^{3+} (RE = La, Gd, Y; Ln = Eu, Tb)

Jun-Lin Yuan[a,b], Zhi-Jun Zhang[a,b], Xiao-Jun Wang[a,b], Hao-Hong Chen[a], Jing-Tai Zhao[a,*], Guo-Bin Zhang[c], Chao-Shu Shi[c]

[a]*State Key Laboratory of High Performance Ceramics and Superfine Microstructure, Shanghai Institute of Ceramics, Chinese Academy of Sciences, Shanghai 200050, PR China*
[b]*Graduate School of Chinese Academy of Sciences, Beijing, PR China*
[c]*NSRL, University of Science and Technology of China, Hefei 230027, PR China*

Received 10 November 2006; received in revised form 22 January 2007; accepted 24 January 2007
Available online 16 February 2007

Abstract

Three rare earth borosilicate oxyapatites, $RE_5Si_2BO_{13}$ (RE = La, Gd, Y), were synthesized via wet chemical method, of which $RE_5Si_2BO_{13}$ (RE = Gd, Y) were first reported in this work. In the three oxyapatites, [BO_4] and [SiO_4] share the [TO_4] tetrahedral oxyanion site, and RE^{3+} ions occupy all metal sites. The differential scanning calorimetry–thermo gravimetry measurements and high temperature powder X-ray diffraction pattern revealed a vitrification process within 300–1200 °C, which was due to the glass-forming nature of borosilicates. From the VUV excitation spectra of Eu^{3+} and Tb^{3+} in $RE_5Si_2BO_{13}$, the optical band gaps were found to be 6.31, 6.54 and 6.72 eV for $RE_5Si_2BO_{13}$ (RE = La, Gd, Y), respectively. The emission and excitation bands of Eu^{3+} and Tb^{3+} are discussed relating with their coordination environments. Among the three hosts, $Y_5Si_2BO_{13}$ would be the best for Eu^{3+} and Tb^{3+}-doped phosphors.
© 2007 Elsevier Inc. All rights reserved.

PACS: 61.66.Fn; 65.40.−b; 78.55.−m

Keyword: Borosilicate; Apatite; Rare earth; VUV spectroscopy

1. Introduction

Apatites constitute a vast family of compounds with the formula of $M_{10}(TO_4)_6X_2$, in which M is metal ion, [TO_4] is tetrahedral oxyanion such as [SiO_4], [PO_4], [VO_4], and X is anion (halide ion, OH, O, S) in the tunnel along c-axis [1–5]. Apatites have long been established as useful luminescent and laser materials [6–8]. In most of the reported apatites the [TO_4] groups are [SiO_4], [PO_4], [VO_4] and [GeO_4]. In 2000, Mazza et al. [9] reported the synthesis of the first rare earth borosilicate oxyapatite, $La_5Si_2BO_{13}$, in which cation sites (4*f* and 6*h* sites) are fully occupied by La^{3+}, [SiO_4] and [BO_4] share the [TO_4] sites, and the charge balance is maintained by the presence of O^{2-} in the tunnel site. However, the structure of isomorphous rare earth borosilicate oxyapatites, thermal stability, and luminescent properties of rare earth doping remain unreported. In this work, two new rare earth borosilicate oxyapatites, $RE_5Si_2BO_{13}$ (RE = Gd, Y), were synthesized, their thermal stability was studied using DSC–TG analysis and high temperature X-ray diffraction (XRD) method, and the Ln^{3+} (Ln = Eu, Tb) doped VUV–UV spectroscopic properties were reported.

*Corresponding author. Fax: +86 021 52413122.
E-mail address: jtzhao@mail.sic.ac.cn (J.-T. Zhao).

0022-4596/$ - see front matter © 2007 Elsevier Inc. All rights reserved.
doi:10.1016/j.jssc.2007.01.033

2. Experimental sections

2.1. Synthesis

Due to the volatile nature of B_2O_3 at high temperature, wet chemical route described by Mazza et al. [9] was adopted to prepare $RE_5Si_2BO_{13}$ (RE = La, Gd, Y) powder samples. The synthesis procedure was described in Fig. 1, in which rare earth oxide was used as the starting material, and the temperature of final heat treatment was 1200 °C rather than 1100 °C reported by Mazza et al. because samples heat treated at 1200 °C showed better crystalline quality than that treat at 1100 °C.

2.2. Characterization

The powder XRD data was collected at ambient temperature with a Rigaku D/max2550 diffractometer (Cu $K\alpha$ radiation, 40 kV/200 mA). A least-square refinement of the observed data was carried out to give the final unit cell parameters. The high-temperature powder XRD data was collected with a multipurpose high temperature attachment on a Rigaku D/max2200 diffractometer (Cu $K\alpha$ radiation, 40 kV/40 mA, Pt sample holder). Differential scanning calorimetry (DSC) and thermo gravimetry (TG) measurements were conducted using a Netzsch STA 409 PC/PG apparatus at a scan rate of 10 °C/min under a flux of N_2.

UV–VIS absorption spectra were recorded on a Shimadzu UV-3101 spectrophotometer equipped with an integrating sphere, using $BaSO_4$ as reference. UV luminescence spectra were recorded on a Shimadyn RF-5301 spectrofluorophotometer at room temperature and a 450 W xenon lamp was used as an excitation source. The VUV excitation and emission spectra were measured at the VUV spectroscopy experimental station on beam line U24 of the National Synchrotron Radiation Laboratory (NSRL), University of Science and Technology of China (USTC). The electron energy of the storage ring was 800 MeV and the beam current was about 150–250 mA with a lifetime of approximately 10 h. The synchrotron radiation was monochromatized through a Seya-Namioka monochromator and the signal was received by a Hamamatsu H5920-01 photomultiplier. The resolution of the instruments is about 0.2 nm. The relative VUV excitation intensities of the samples are corrected by dividing the measured excitation intensities of the samples with that of sodium salicylate in the same excitation conditions. All of the excitation and emission spectra are recorded at room temperature.

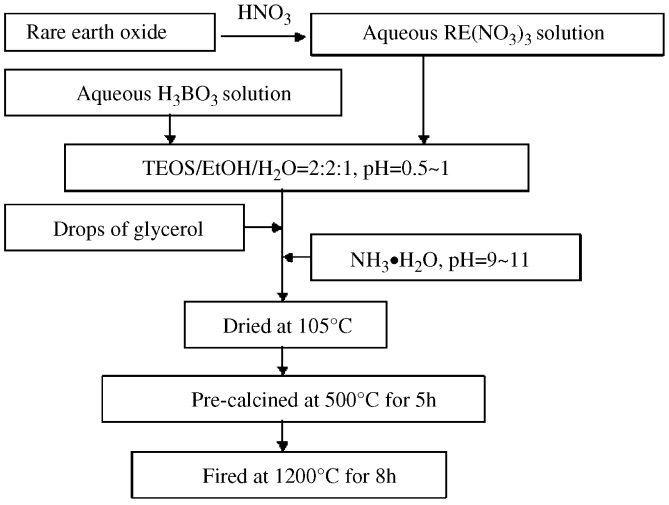

Fig. 1. Wet chemical procedure of preparing $RE_5Si_2BO_{13}$ (RE = La, Gd, Y) powder samples.

3. Results and discussion

3.1. Crystal structure of $RE_5Si_2BO_{13}$ (RE = La, Gd, Y)

The XRD patterns of $RE_5Si_2BO_{13}$ (RE = La, Gd, Y) are given in Fig. 2, which can be successfully indexed using TREOR method integrated in *FullProf* [10]. The unit cell parameters refined are presented in Table 1, together with the unit cell parameters of $La_{9.33}Si_6O_{26}$ (RE = La, Gd, Y). The XRD peaks of $RE_5Si_2BO_{13}$ (RE = Gd, Y) are tabulated in Table 2. Due to the smaller radii of Gd^{3+} (105 pm) and Y^{3+} (102 pm) relative to La^{3+} (116 pm) [11], the unit cell parameters reduce as Gd^{3+} and Y^{3+} totally replace La^{3+}. Nevertheless, such equivalent charge substitution with small RE^{3+} destabilizes the borosilicate oxyapatite structure, which is indicated by the minute amount of Y_2SiO_5 second phase (Fig. 2). As a matter of fact, in trying to synthesize $RE_5Si_2BO_{13}$ (RE = Tm, Yb, Lu) under the same experimental conditions, RE_2SiO_5 and $REBO_3$ were obtained instead. As will be shown in Section 3.3, the extra yttrium silicate phase in $Y_5Si_2BO_{13}$

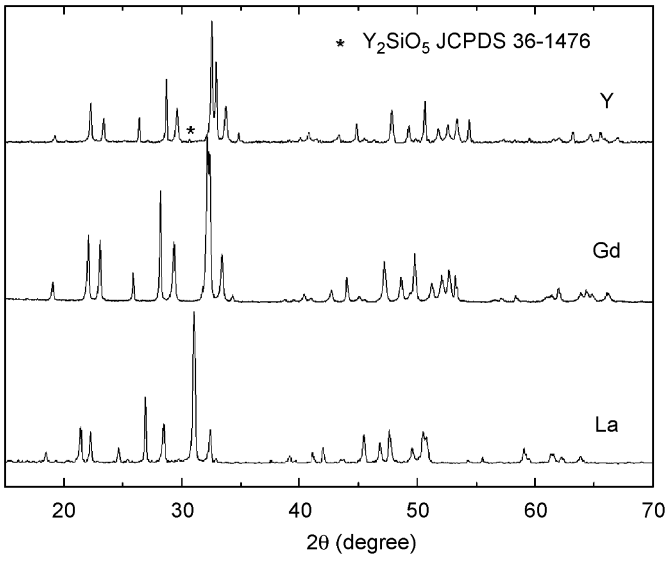

Fig. 2. XRD patterns of $RE_5Si_2BO_{13}$ (RE = La, Gd, Y) powder samples. The weak extra peak at 30.7° in the XRD pattern of $Y_5Si_2BO_{13}$ indicates the presence of Y_2SiO_5 phase.

Table 1
Refined unit cell parameters of $RE_5Si_2BO_{13}$ (RE = Y, La, Gd), in comparison with rare earth silicate oxyapatites. For $RE_5Si_2BO_{13}$, S.G. $P6_3/m$ (no. 176), $Z = 2$

	a (Å)	c (Å)	Vol. (Å^3)	D_{cal} (g/cm^3)	F. O. M.	Reference
$La_5Si_2BO_{13}$	9.5620	7.2149	571.30	5.64	$F(29) = 37.0$ (0.014, 55)	This work
$Gd_5Si_2BO_{13}$	9.2835	6.8758	513.19	6.87	$F(30) = 81.8$ (0.009, 43)	This work
$Y_5Si_2BO_{13}$	9.1934	6.7392	493.27	4.85	$F(30) = 73.2$ (0.011, 39)	This work
$La_5Si_2BO_{13}$	9.5587	7.2173	571.09	5.64		[9]
$La_{9.33}Si_6O_{26}$	9.713	7.186	587.08	5.32		JCPDS No. 49-0443
$Gd_{9.33}Si_6O_{26}$	9.4264	6.8444	526.69	6.468		JCPDS No. 38-0283
$Y_{9.33}Si_6O_{26}$	9.347	6.727	508.98	4.62		JCPDS No. 30-1457

Table 2
X-ray diffraction peaks for (a) $Gd_5Si_2BO_{13}$ and (b) $Y_5Si_2BO_{13}$

$2\theta_{obs}$	$2\theta_{cal}$	hkl	Intensity	$2\theta_{obs}$	$2\theta_{cal}$	hkl	Intensity
(a)							
32.177	32.180	211	100	48.642	48.630	312	15.6
32.370	32.380	112	89.4	19.081	19.105	110	12.9
28.201	28.209	102	65.4	51.256	51.239	321	12.4
22.074	22.095	200	39.3	61.982	61.975	214	9.5
23.084	23.100	111	38.2	64.343	64.333	304	8.3
29.359	29.368	210	37.1	42.745	42.747	302	8.1
33.405	33.409	300	29.5	63.857	63.857	502	6.7
49.795	49.792	213	29.1	49.375	49.370	320	6.2
47.218	47.213	222	24.0	66.139	66.179	332	6.2
52.718	52.711	402	20.3	64.867	64.833	323	5.6
25.890	25.895	002	18.2	40.421	40.419	310	5.5
52.091	52.088	410	17.0	61.376	61.367	331	5.1
53.258	53.247	004	16.4	58.332	58.336	204	5.0
44.026	44.028	113	15.7	34.296	34.294	202	4.8
(b)							
32.564	32.561	211	100	44.879	44.873	113	14.3
32.937	32.932	112	67.9	51.846	51.818	321	11.8
28.744	28.746	102	54.8	65.599	65.580	304	9.2
22.307	22.314	200	34.8	34.848	34.856	202	9.0
33.752	33.746	300	31.6	63.205	63.200	214	8.8
50.677	50.670	213	31.5	40.846	40.833	310	8.7
29.651	29.663	210	30.8	19.278	19.294	110	7.3
47.870	47.869	222	26.2	64.734	64.694	502	7.2
26.424	26.430	002	23.1	43.379	43.366	302	6.7
23.403	23.407	111	21.5	67.019	67.045	332	5.2
53.422	53.392	303	18.8	62.044	62.070	331	4.9
54.419	54.414	004	17.0	49.892	49.887	320	4.8
52.639	52.638	410	15.1	40.129	40.144	212	4.7
49.320	49.300	312	14.4	61.553	61.588	420	4.0

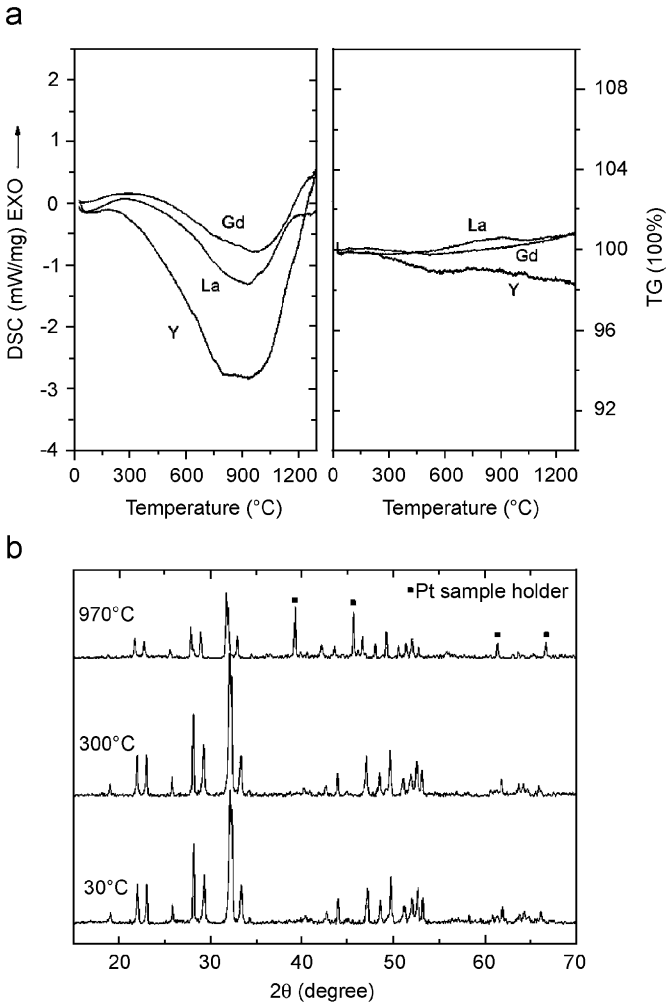

Fig. 3. (a) DSC–TG measurements of $RE_5Si_2BO_{13}$ (RE = La, Gd, Y) and (b) powder XRD patterns $Gd_5Si_2BO_{13}$ at different temperatures.

samples is not rich enough to interfere the luminescent spectra because $Y_5Si_2BO_{13}$ is also a good host for Eu^{3+} and Tb^{3+}.

3.2. Thermal stability

From the DSC–TG measurements from room temperature to 1300 °C (Fig. 3a), $RE_5Si_2BO_{13}$ (RE = La, Gd, Y) present similar thermal stability features: no obvious weight loss and a very broad endothermal band from 300 to 1200 °C. Due to the similarities in structure and DSC–TG curves in the series of $RE_5Si_2BO_{13}$ (RE = La, Gd, Y), high temperature XRD pattern of $Gd_5Si_2BO_{13}$ was recorded to study the nature of broad endothermal band around 1000 °C (Fig. 3b). The $Gd_5Si_2BO_{13}$ apatite phase can be stable around 1000 °C, but the relative weak diffraction peaks of $Gd_5Si_2BO_{13}$ and the presence of Pt peaks suggest a melting process at the maximum point of endothermal band. Besides, samples air-quenched from 1200 °C showed no perceptible difference from that of

samples cooled naturally with the furnace. Considering the glass-forming nature of borosilicates, the broad endothermal band in DSC might be attributed to a vitrification process that occurred in the range from 300 to 1200 °C, and the rate of crystallization from glass is very fast [12]. The thermal expansion coefficients of $Gd_5Si_2BO_{13}$ apatite were estimated to be 1.23×10^{-4} Å K^{-1} and 6.83×10^{-5} Å K^{-1} along the *a*- and *c*-axis, respectively.

3.3. VUV–UV spectroscopic properties of RE5Si2BO13:Ln3+ (RE = La, Gd, Y; Ln = Eu, Tb)

There are two metal sites in apatite: 4*f* site (CN = 9, C_3) and 6*h* site (CN = 7, C_s). The 4*f* site cation connects with 6 ionic $[TO_4]$ (X = P, Si, B, V…) oxyanions, but the 6*h* site cation also coordinated to the free O^{2-} anion in the tunnel at a very short distance. It has been established that crystal field at both sites are of comparable strength [13], but the activators at 6*h* sites would be influenced by larger covalent component in bonding with the free O^{2-} [14,15]. For example, shorter length and more covalent of the Eu^{3+}–O^{2-} bond will considerably shift the position of charge transfer band (CTB) towards low energy side [16]; more covalent bonding with the free O^{2-} ion would drastically lowers the position of the lowest 4*f*5*d* level of RE^{3+} (*RE* = Ce, Pr, Tb…) [17]. Consequently, comparing with the activators at 4*f* site, activators at 6*h* site will make greater contribution to the optical properties that related to CTS and the lowest 4*f*5*d* band.

$RE_5Si_2BO_{13}$ (*RE* = La, Gd, Y) are transparent from visual region up to about 220 nm (Fig. 4), suggesting that $RE_5Si_2BO_{13}$ (*RE* = La, Gd, Y) are appropriate hosts of rare earth ion (such as Eu^{3+} and Tb^{3+}) doped luminescent materials. The VUV–UV excitation spectra and emission spectra of Eu^{3+}/Tb^{3+}-doped samples are presented in Fig. 5. The moderate bands within 160–200 nm in the excitation spectra of both Eu^{3+} and Tb^{3+} can be identified as the host absorption bands, from which the optical band gap of $RE_5Si_2BO_{13}$ (*RE* = La, Gd, Y) are calculated to be 6.31, 6.54 and 6.72 eV, respectively. The optical band gaps of $RE_5Si_2BO_{13}$ (*RE* = La, Gd, Y) are smaller than that of the corresponding silicates and borates such as RE_2SiO_5 and $REBO_3$ [18], which could be attributed to the presence of free O^{2-} ions in apatite structures.

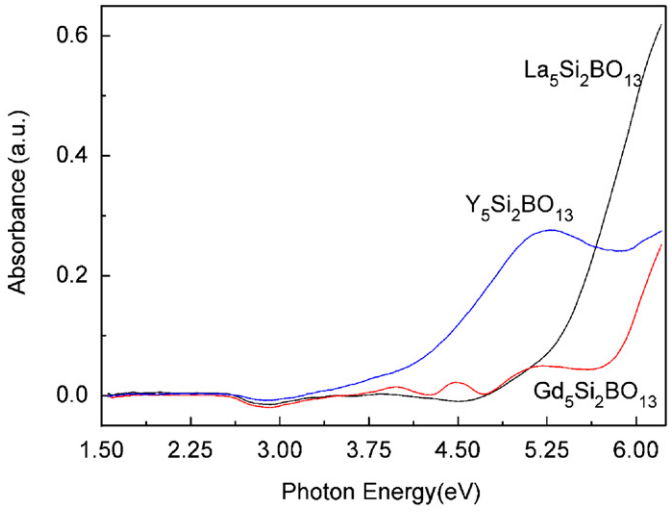

Fig. 4. Room temperature absorption spectra of $RE_5Si_2BO_{13}$ (*RE* = La, Gd, Y) powder samples. The host absorption edge of $Y_5Si_2BO_{13}$ may be higher than 6.2 eV, which is the high-energy limit of the apparatus.

As shown in Fig. 5, both excitation and emission spectra of Ln^{3+} (*Ln* = Eu, Tb) feature principally the same curve shape through the series of $RE_5Si_2BO_{13}$ (*RE* = La, Gd, Y), which would be a strong evidence for the isomorphous nature of the three hosts. For Eu^{3+}-doped sample, the excitation spectra is dominated by a broad CTB of Eu^{3+}–O^{2-} within 200–350 nm, together with the host absorption band within 175–200 nm. It has been proved that in Eu^{3+}-doped $Sr_2La_8(GeO_4)_6O_2$ apatites, the CTS and $^7F_0$–$^5D_2$ excitation at 464 nm can be more effective to excite the Eu^{3+} at 6*h* site, and the $^7F_0$–$^5L_6$ excitation at 394 nm is more effective to Eu^{3+} at 4*f* sites [19]. Similar assignments can be obtained by comparing with the emission spectra under different excitations as shown in Fig. 6. Besides, the positions of Eu^{3+} CTB in $RE_5Si_2BO_{13}$ resemble with that in RE_2O_3 (*RE* = La, Gd, Y) hosts [20], but are energetically lower than that of Eu^{3+} in rare earth orthosilicates and orthoborates [18], which confirms the great contribution made by $O^{2-}\rightarrow Eu^{3+}$ (6*h*) CT process to the observed CTB. As for the Eu^{3+} at 4*f* site, the CTB is less efficient and might be hidden in the high-energy side of the observed CTB. Nevertheless, distinguish of 4*f* from 6*h* in the CTB seems unlikely due to the very broad nature of CTB. In the emission spectra under CTB excitation (Fig. 6), the $^5D_0$–$^7F_0$ transition at 580 nm is moderately strong, and the intensity of electric-dipole $^5D_0$–$^7F_2$ transition is stronger than that of magnetic-dipole $^5D_0$–$^7F_1$ transition, verifying the fact that Eu^{3+} ions stay at sites without inverse symmetry.

As for Tb^{3+} doped samples, the excitation spectra are featured as moderate host absorption band below 200 nm and strong Tb^{3+} 4*f*–5*d* spin-allowed bands within 200–260 nm, and the strongest $^5D_4$–$^7F_5$ emissions around 544 nm in the emission spectra. At least three Tb^{3+} 4*f*–5*d* spin-allowed bands can be identified in the excitation spectra (Table 3). As stated above, crystal field at both 4*f* and 6*h* sites are of comparable strength [13], but the 4*f*5*d* levels of Tb^{3+} at 6*h* sites would be suppressed by greater covalency in bonding with the free O^{2-} ion. Therefore, the lowest 4*f*–5*d* spin-allowed band is assigned as Tb^{3+} at 6*h* sites. Furthermore, in Ce^{3+}-doped $Ln_{9.33}(SiO_4)_6O_2$ (*Ln* = La, Gd) oxyapatites, the lowest and second 4*f*5*d* band in the excitation band of Ce^{3+} was attributed to Ce^{3+} ion at 6*h* site and 4*f* site, respectively [21]. Due to the similar 4*f*5*d* energy structures and simple energy shift relationship between Tb^{3+} and Ce^{3+} [22], the second lowest 4*f*–5*d* spin-allowed band is tentatively attributed to be Tb^{3+} at 4*f* sites (Fig. 5a). Tb^{3+} 4*f*–5*d* bands in these

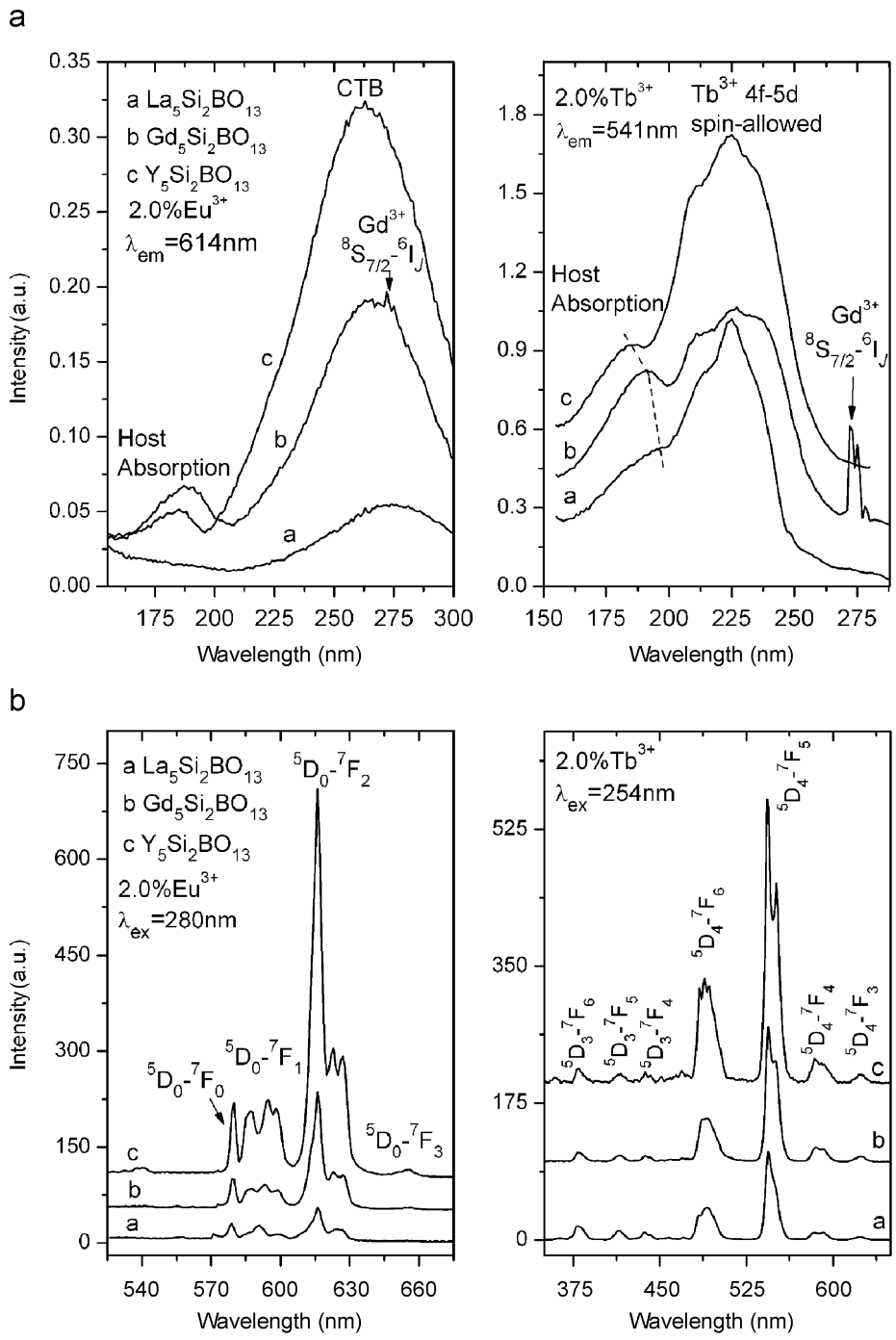

Fig. 5. (a) Room temperature VUV–UV excitation spectra, and (b) UV-excited emission spectra of Eu^{3+} and Tb^{3+}-doped $RE_5Si_2BO_{13}$ (RE = La, Gd, Y) samples.

three hosts are at lower energy positions relative to that in $Ln_{9.33}(SiO_4)_6O_2$ (Ln = La, Gd) [21], suggesting that the partial substitution of Si with B has increased the crystal field intensity at 6*h* site, which may be brought out by two factors: the reduced size of [LnO_n] polyhedron and more covalency in the free O^{2-} ion [15] due to the partial substitution of Si with B.

On the other side, due to the high sensitivity of optical properties with local coordination environment [23], the structure evolution with decreasing ionic radii from La^{3+} to Y^{3+} also brings notable spectroscopic difference in $RE_5Si_2BO_{13}$:Ln^{3+} (RE = La, Gd, Y; Ln = Eu, Tb). For example, the position and relative intensity of Eu^{3+} CTB and Tb^{3+} 4*f*–5*d* bands, the relative emission intensity from difference emission levels. Firstly, Eu^{3+}-doping was examined. The energy of CTB in $RE_5Si_2BO_{13}$ hosts follows the sequence of $E_{Eu}^{CT}(Y) > E_{Eu}^{CT}(Gd) > E_{Eu}^{CT}(La)$ (Table 3), following sequence of electronegativity of RE^{3+}

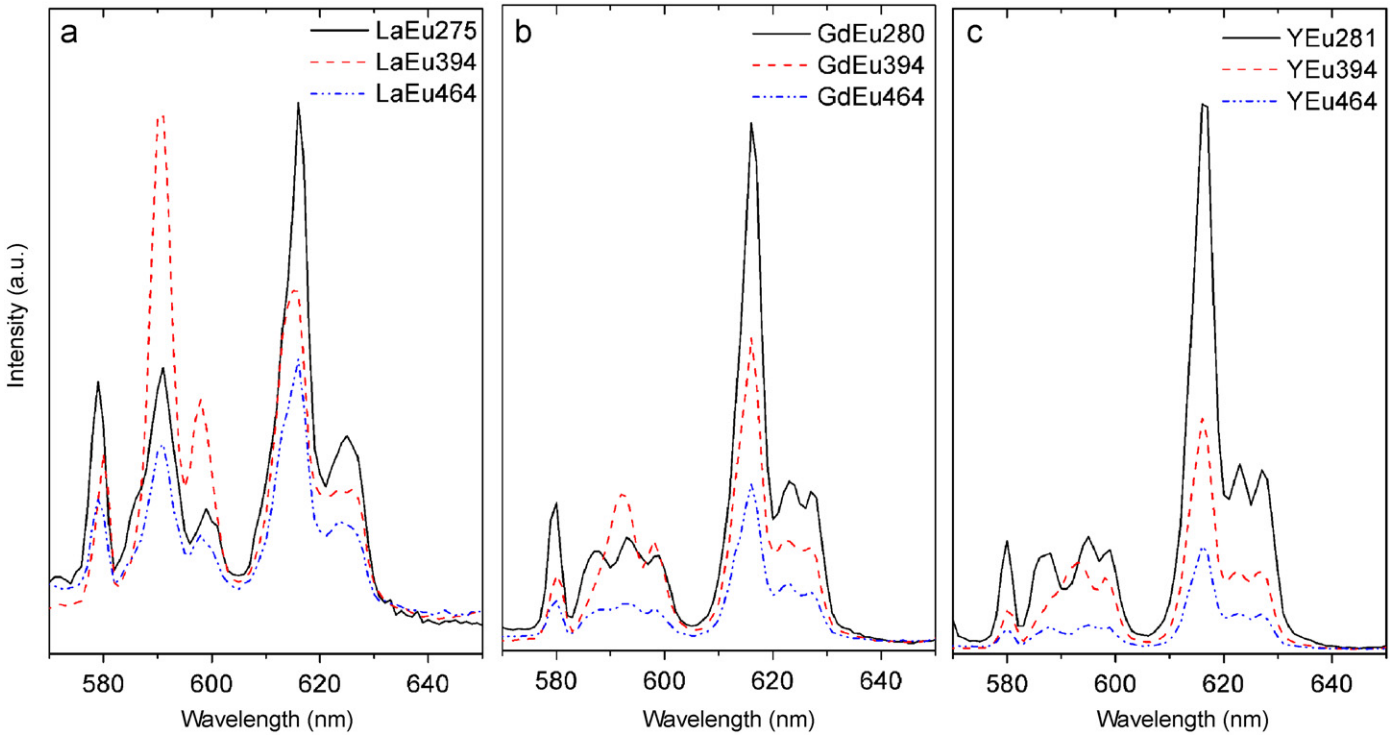

Fig. 6. The luminescent spectra of 2.0%Eu^{3+}-doped $RE_5Si_2BO_{13}$ samples under CTS (~280 nm), $^7F_0$–$^5L_6$ (394 nm) and $^7F_0$–$^5D_2$ (464 nm) excitations.

Table 3
Positions of excitation bands of Eu^{3+} and Tb^{3+}-doped $RE_5Si_2BO_{13}$

$RE_5Si_2BO_{13}$	$La_5Si_2BO_{13}$	$Gd_5Si_2BO_{13}$	$Y_5Si_2BO_{13}$
Host absorption peak (nm)	197	190	185
Eu^{3+} CTB (nm)	276	268	263
Tb^{3+} 4f–5d (nm)	238,227,214	230, 227, 214	236, 223, 211

$\chi_Y(1.22) > \chi_{Gd}(1.20) > \chi_{La}(1.11)$ [24]. The remarkable difference in the CTB intensity can be discussed in configurational coordination diagram (Fig. 7) [6]: For Eu^{3+} ions, the relaxation space in $La_5Si_2BO_{13}$ is the largest, and the smallest in $Y_5Si_2BO_{13}$, leading to a relatively large offset of CTB parabola in $La_5Si_2BO_{13}$ and a small offset in $Y_5Si_2BO_{13}$. As a result, in $La_5Si_2BO_{13}$:Eu^{3+} a major part of energy is lost via non-radiative CTB→^7F_J relaxation (process 3 in Fig. 7) and in $Y_5Si_2BO_{13}$:Eu^{3+} most of the energy is released by emitting red photons (processes 2 and 4 in Fig. 7). In the emission spectra excited at CTB, the $I(^5D_0$–$^7F_2)/I(^5D_0$–$^7F_1)$ integration intensity increases in the La→Gd→Y sequence, suggesting the more and more stronger parity-mixing effect at 6*h* site [15].

As for Tb^{3+}-doped samples, the Tb^{3+} emission intensity increases steadily but the percentage of emissions from $^5D_3$ level decreases gradually when the Tb^{3+} concentration increases from 2.0% to 10.0% (Fig. 8), which indicate that the optimal Tb^{3+} concentration in the three hosts may be beyond 10.0%, and the cross-quenching process of $^5D_3$ emissions gets more and more prominent as the Tb-Tb distance decreases [6]. The $^5D_3$ quenching effect is less

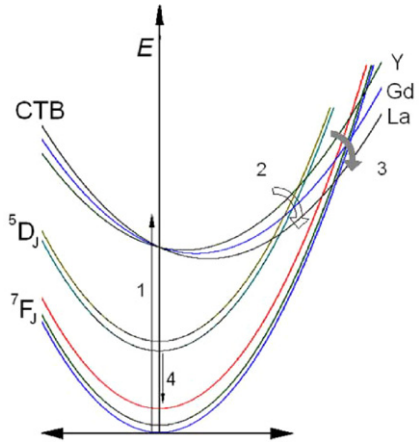

Fig. 7. Configurational coordination diagram of Eu^{3+} emission excited at CTB. 1 is excitation at CTB, 2 is relaxation from CTB to excited ^5D_J levels that leads to radiative relaxation to ^7F_J levels, and 3 is non-radiative relaxation from CTB to ground level.

evident in $La_5Si_2BO_{13}$ due to its larger unit cell parameters and longer Tb–Tb intercation distances. In $RE_5Si_2BO_{13}$ (RE = La, Gd, Y), RE^{3+} ions at 4*f* sites form a linear chain along *c*-axis with inter-cation distance of 0.5*c*, which is the shortest RE^{3+}–RE^{3+} distance in $RE_5Si_2BO_{13}$ oxyapatites. Since most of the multi-dipole energy transfer rates between activators are very sensitive to donor–acceptor distance, the RE^{3+} ion chain at 4*f* sites would be a preferential channel for fast energy transfer comparing with energy transfer occur between 6*h*–6*h* and 4*f*–6*h* activator pairs.

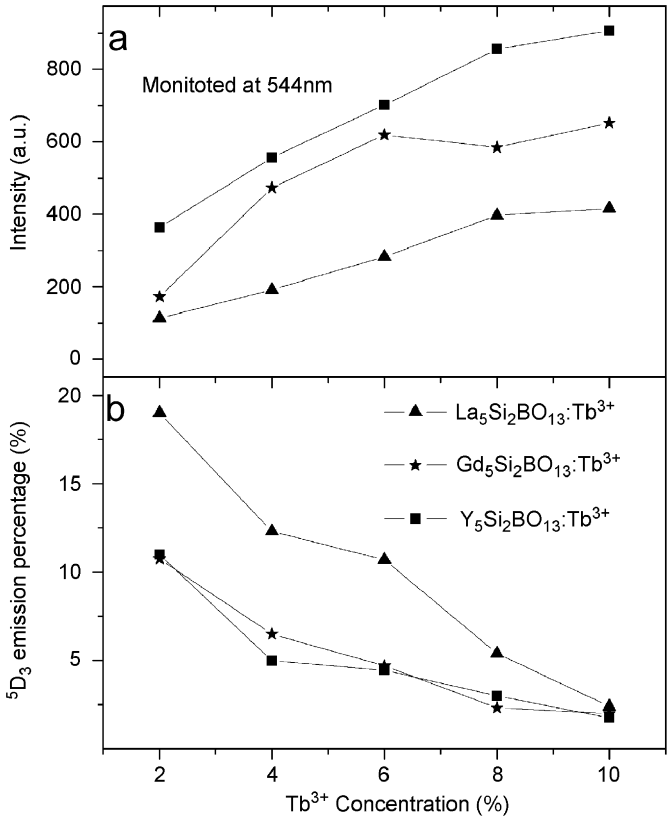

Fig. 8. (a) The emission intensity monitored at 544 nm and (b) the percentage of $^5D_3$ emission of $RE_5Si_2BO_{13}:x\%Tb^{3+}$ (RE = La, Gd, Y; x = 2.0, 4.0, 6.0, 8.0, 10.0) samples. The excitation wavelength is 254 nm.

4. Conclusions

In this work, three rare earth borosilicate oxyapatites $RE_5Si_2BO_{13}$ (RE = La, Gd, Y) were synthesized, their thermal stability and Eu^{3+}/Tb^{3+}-doped VUV–UV spectroscopic properties were studied. The DSC–TG measurement and high temperature XRD reveal a vitrification transition from 300 to 1200 °C, which was due to the glass-forming nature of borosilicates. From the host absorption bands identified in the excitation spectra, the optical band gaps were found to be 6.31, 6.54 and 6.72 eV for $RE_5Si_2BO_{13}$ (RE = La, Gd, Y), respectively. It was observed that the free O^{2-} anion is closely related with the Eu^{3+} CTB and the lowest 4*f*5*d* band of Tb^{3+}. Besides, comparing with B-free rare earth silicate oxyapatites, the partial substitution of Si with B has significantly increased the intensity of crystal field at both 4*f* and 6*h* sites. Among the three hosts, $Y_5Si_2BO_{13}$ would be the best for both Eu^{3+} and Tb^{3+} activators.

Acknowledgment

This work was supported by the Key Project (50332050) from the NNSF of China, the Hundred Talents Program from the Chinese Academy of Sciences, Fund for Young Leading Researchers from Shanghai municipal government. Special thanks are given to Dr. J.F. Zhu and Prof. Y.J. Zhu for DSC–TG measurements.

References

[1] K. Sudarsanan, R.A. Young, Acta Cryst. B 25 (1969) 1534–1543.
[2] L.L. Boyer, P.A. Fleury, Phys. Rev. B 9 (1974) 2693–2700.
[3] Th. Leventouri, C.E. Bunaciu, V. Perdikatsis, Biomaterials 24 (2003) 4205–4211.
[4] R.E. Ouenzerfi, M.-T. Cohen-Adad, C. Goutaudier, G. Panczer, Solid State Ionics 176 (2005) 225–231.
[5] H. Okudera, Y. Masubuchi, S. Kikkawa, A. Yoshiasa, Solid State Ionics 176 (2005) 1473–1478.
[6] G. Blasse, B.C. Grabmaier, Luminescent Materials, Springer, Berlin, Heidelberg, 1994.
[7] C. Feldmann, T. Jüstel, C.R. Ronda, P.J. Schmidt, Adv. Funct. Mater. 13 (2003) 511–518.
[8] A. Yoshikawa, F. Fujiwara, H. Sato, T. Nishi, H. Ohta, T. Fukuda, Y. Waseda, G. Boulon, M. Ito, Y. Guyot, K. Lebbou, Opt. Mater. 26 (2004) 385–390.
[9] D. Mazza, M. Tribaudino, A. Delmastro, B. Lebech, J. Solid State Chem. 155 (2000) 389–393.
[10] J. Rodriguez-Carvajal, FULLPROF: A Program for Rietveld Refinement and Pattern Matching Analysis, Abstracts of the Satellite Meeting on Powder Diffraction of the XV Congress of the IUCr, Toulouse, France, 1990, p. 127.
[11] A. Kelly, G.W. Groves, Crystallography and Crystal Defects, Addison-Wesley, Reading, MA, 1970.
[12] I. Kratochvilova-Hruba, I. Gregora, J. Pokorny, S. Kamba, Z. Zikmund, J. Petzelt, M. Cernansky, V. Studnicka, V.N. Sigaev, E.N. Smelyanskaya, J. Non-Cryst. Solids 290 (2001) 224–230.
[13] G. Blasse, J. Solid State Chem. 14 (1975) 181.
[14] N. Lakshminarasimhan, U.V. Varadaraju, J. Solid State Chem. 177 (2004) 3536–3544.
[15] L. Boyer, B. Piriou, J. Carpena, J.L. Lacout, J. Alloy. Compd. 311 (2000) 143–152.
[16] P. Dorenbos, J. Phys.: Condens. Matter. 15 (2003) 8417–8434.
[17] P. Dorenbos, Phys. Rev. B 64 (2001) 125117–125129.
[18] Y.H. Wang, X. Guo, T. Endo, Y. Murakami, M. Ushirozawa, J. Solid State Chem. 177 (2004) 2242–2248.
[19] Y.C. Li, Y.H. Chang, B.S. Tsai, Y.C. Chen, Y.F. Lin, J. Alloy. Compd. 416 (2005) 199–205.
[20] L.D. Sun, C.S. Liao, C.H. Yan, J. Solid State Chem. 171 (2003) 304–307.
[21] M.J.J. Lammers, G. Blasse, J. Electrochem. Soc. 134 (1987) 2068–2072.
[22] P. Dorenbos, J. Lumin. 91 (2000) 155–176.
[23] R. Jagannathan, M. Kottaisamy, J. Phys.: Condens. Mater. 7 (1995) 8453–8466.
[24] L.C. Allen, J. Am. Chem. Soc. 111 (1989) 9003.